Quantum Inf Process
DOI 10.1007/s11128-016-1489-3

Emulation of complex open quantum systems using superconducting qubits

Sarah Mostame[1,4] · Joonsuk Huh[1,5] · Christoph Kreisbeck[1] · Andrew J. Kerman[2] · Takatoshi Fujita[1,6] · Alexander Eisfeld[3] · Alán Aspuru-Guzik[1]

Received: 21 April 2016 / Accepted: 10 October 2016

Abstract With quantum computers being out of reach for now, quantum simulators are alternative devices for efficient and accurate simulation of problems that are challenging to tackle using conventional computers. Quantum simulators are classified into analog and digital, with the possibility of constructing "hybrid" simulators by combining both techniques. Here we focus on analog quantum simulators of open quantum systems and address the limit that they can beat classical computers. In particular, as an example, we discuss simulation of the chlorosome light-harvesting antenna from green sulfur bacteria with over 250 phonon modes coupled to each electronic state. Furthermore, we propose physical setups that can be used to reproduce the quantum dynamics of a standard and multiple-mode Holstein model. The proposed scheme is based on currently available technology of superconducting circuits consist of flux qubits and quantum oscillators.

Keywords Quantum information · Quantum algorithms and protocols · Quantum interference devices · Superconducting circuits · Quantum simulation · Photochemistry

✉ Sarah Mostame
sarah.mostame@intel.com

1 Department of Chemistry and Chemical Biology, Harvard University, Cambridge, MA 02138, USA

2 Lincoln Laboratory, Massachusetts Institute of Technology, Lexington, MA 02420, USA

3 Max-Planck-Institut für Physik komplexer Systeme, Nöthnitzer Str. 38, 01187 Dresden, Germany

4 Present Address: Intel Labs, 2111 NE 25th Avenue, Hillsboro, OR 97124, USA

5 Present Address: Mueunjae Institute for Chemistry (MIC), Department of Chemistry, Pohang University of Science and Technology (POSTECH), Pohang 790-784, Korea

6 Present Address: Institute of Molecular Science, Okazaki, Japan

Published online: 28 December 2016

1 Introduction

There is a growing interest in understanding the dynamics of open quantum systems, particularly, when particles or quasiparticles are coupled to a vibrational environment. Such situations arise in quantum chemistry and condensed matter physics, for example, in photosynthetic complexes or molecular aggregates. Thus, a detailed study of the dynamics of electron–phonon interaction becomes desirable. Although many analytical and numerical methods have been employed to simulate this problem [1–13], their applicability is often limited by the number of the phonon modes coupled to the electronic states or to a particular investigation (e.g., low-lying excited polaron) and a specific parameter regime. The resources required for most of the classical computational methods increase exponentially with the number of particles in the simulation, and it is challenging to simulate the dynamics of open quantum systems on conventional computers, even using modern parallel processing units [14–16].The situation becomes even much more challenging for complex open quantum systems with structured environments. As yet, only small model systems have been studied theoretically with crude approximations to the system-bath dynamics, see for example [17,18]. Numerically exact solution can be obtained for only small systems ($<$20 sites) with restrictions on the bath modes [14,16,19–22]. State-of-the-art massively parallelized implementations of the hierarchically coupled equation of motion (HEOM) approach [14,16,23] have proven as one of the most efficient methods (with respect to both system size and complexity of the spectral density) to accurately acquire the quantum dynamics of the Holstein model. In Fig. 1, we estimate the upper limit for simulating such complex open quantum systems with current computational resources on conventional computers. Here, we use *QMaster* [16] as a benchmark. The horizontal axis indicates the system size (number of the particles or sites) that can be simulated while the vertical axis indicates number of the peaks in the spectral density that could be considered in this simulation, see Ref. [16] for more computational details. Note that "peaks" here refers to Drude–Lorentz peaks in the spectral density [16] which should not be confused with the number of phonon modes in the Hamiltonian. Each of these peaks in the spectral density may include several phonon modes. Further details are given in "Appendices 2 and 3."

In this work, we propose analog quantum devices [24–29] to mimic the dynamics of complex open quantum systems and demonstrate that they can be constructed using present-day technology of superconducting circuits and outperform current classical computational methods. With such quantum simulators, one can perform more extensive investigation including exciton transport, spectral density, absorption spectra as well as wide range of parameters and thereby a more detailed understanding of the problems. Furthermore, our proposed quantum simulators occupy a wide region in the plot shown in Fig. 1. Similar ideas for simulating Holstein polarons based on polar molecules trapped in an optical lattice [30,31], Rydberg states of cold atoms and ions [32], trapped ions [33,34], and superconducting circuit quantum electrodynamics (QED) [35,36] have been pursued earlier. However, the main focus of this paper is emulating the dynamics of multiple-mode Holstein models at finite temperature—with application in open quantum systems with complex environments—which has not been addressed in any of the above mentioned references. Moreover, it is worth-

while to study an alternative setup, since different experimental realizations carry distinct advantages and drawbacks. For example, the proposal based on trapped ions in Ref. [33], that simulates the standard Holstein model, does not outline how a similar approach can be used to tailor many phonon modes to simulate the structured spectral densities that is the main focus of this paper. Additionally, it is focused on simulating the Holstein model in a parameter regime of strong coupling.

2 Standard Holstein model

We first focus on simulating an electron–phonon model which describes the interaction of a single electron on a 1D finite lattice with one vibrational mode per lattice site, namely the Holstein model:

$$H_{\mathrm{Hol}} = H_{\mathrm{el}} + H_{\mathrm{ph}} + H_{\mathrm{el-ph}} \,. \tag{1}$$

The first term of the Hamiltonian is given by

$$H_{\mathrm{el}} = \sum_{n=1}^{N} \epsilon_n \, a_n^{\dagger} a_n + \sum_{n=1}^{N-1} V_n \left(a_n^{\dagger} a_{n+1} + a_{n+1}^{\dagger} a_n \right) \tag{2}$$

with ϵ_n being the electronic transition energies of site n, V_n being the strength of the nearest-neighbor couplings, $a_n^{\dagger}$ (a_n) being the creation (annihilation) operators of the electron and N being the number of sites. The phonon Hamiltonian

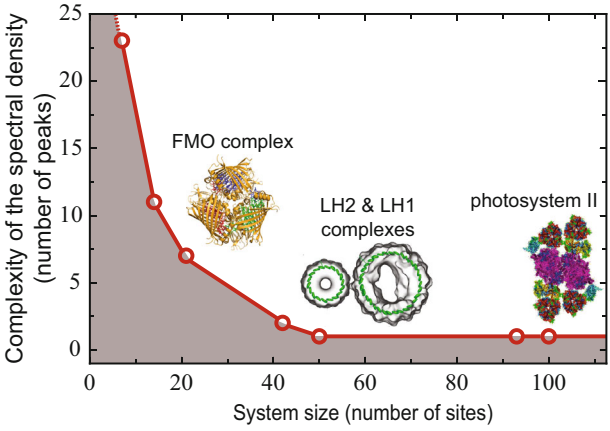

Fig. 1 The *gray* area shows the estimated treatable system sizes for the simulation of Frenkel exciton Hamiltonians using current classical supercomputing resources. There is a trade off between the complexity of the spectral density and the system size that denotes the classically feasible area. Three photosynthetic systems are shown: The Fenna–Mathews Olson (FMO) complex of green sulfur bacteria, the light-harvesting I and II complexes of purple bacteria, and photosystem II of higher plants. The simulation has been performed using the hierarchical equations of motion (HEOM) approach on 64 AMD Opteron cores employing a total of 250 GB of RAM

is $H_{\rm ph} = \sum_{n=1}^{N} \hbar\omega_n b_n^\dagger b_n$, with ω_n being the frequency of the phonon mode coupled to the n-th lattice site and $b_n^\dagger$ (b_n) being the creation (annihilation) operators of the phonon. The last term in Eq. (1) describes the electron–phonon coupling $H_{\rm el-ph} = \sum_{n=1}^{N} \kappa_n\, a_n^\dagger a_n \left(b_n^\dagger + b_n\right)$ with κ_n being the coupling strength between the electron and phonon at lattice site n. Using the Jordan–Wigner transformation, the Hamiltonian $H_{\rm Hol}$ can be rewritten in terms of the Pauli $\boldsymbol{\sigma}$ operators,

$$H_{\rm Hol} = \frac{1}{2}\sum_{n=1}^{N-1} V_n \left(\sigma_x^n \sigma_x^{n+1} + \sigma_y^n \sigma_y^{n+1}\right) + \sum_{n=1}^{N}\left[\frac{\epsilon_n}{2}\,\sigma_z^n + \kappa_n\,\sigma_z^n\left(b_n^\dagger + b_n\right) + \hbar\omega_n b_n^\dagger b_n\right]. \tag{3}$$

In order to reproduce the quantum dynamics of the open system given by the above Hamiltonian, let us consider a chain of N gradiometric flux qubits [27,37] with tunable $\sigma_z\sigma_z$-couplings [38,39] and a single LC oscillator coupled to each qubit, as shown in Fig. 2. The Hamiltonian of a single flux qubit in the bare basis, the quantum states with magnetic flux pointing up $|\uparrow\rangle$ and down $|\downarrow\rangle$, is given by $H_{\rm q}^i = (\mathscr{E}_i\,\sigma_z^i + \Delta_i\,\sigma_x^i)/2$ [40,41], where $\mathscr{E}_i$ is the energy bias between $|\uparrow\rangle$ and $|\downarrow\rangle$, Δ_i is the tunnel splitting between the two states and i labels the position of the qubit in the chain. Note that $\mathscr{E}_i$ can be tuned to zero to neglect the term $\mathscr{E}_i\sigma_z^i$ and therefore be at the optimal operating point [42] of the flux qubit, which is the most common case in current experiments. The coupling between two nearest-neighbor qubits in the bare basis is given by $H_{\rm coup}^i = g_i(\Delta_{ii+1}^c)\,\sigma_z^i\,\sigma_z^{i+1}$, where Δ_{ii+1}^c is the (tunable) tunnel splitting of the coupler qubit (smaller qubits in Fig. 2, see Ref. [27] for more details). The coupling of a quantum LC oscillator to the smaller loop of a flux qubit, as shown in Fig. 2, is given by $H_{\rm q-osc}^i = \eta_i\,\sigma_x^i\left(c_i^\dagger + c_i\right)$ with $c_i^\dagger$ (c_i) being the creation (annihilation) operator of the oscillator coupled to the i-th qubit and η_i being the coupling strength. Finally, the Hamiltonian of a single oscillator is $H_{\rm osc}^i = \hbar\omega_i'\,c_i^\dagger c_i$ with ω_i' being the transition frequency of the oscillator. Rewriting the above Hamiltonians

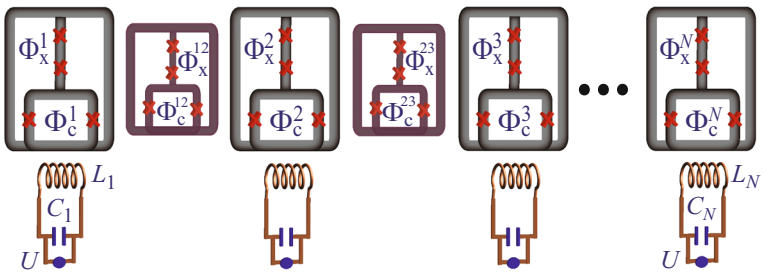

Fig. 2 Superconducting quantum circuit diagram of the proposed quantum simulator for the Holstein model. The qubit states are encoded in the quantized circulating current of the qubit loop. The *red* crosses denote Josephson junctions. The gradiometric flux qubits are coupled with a tunable $\sigma_z\sigma_z$-coupling. Each of the qubits is independently coupled to a quantum LC oscillator to simulate the vibrational environment (Color figure online)

in the energy eigenbasis of the qubit $|\pm\rangle = (|\downarrow\rangle \pm |\uparrow\rangle)/\sqrt{2}$ converts the operators $\sigma_x^i \rightarrow \sigma_z^i$ and $\sigma_z^i \sigma_z^{i+1} \rightarrow \sigma_x^i \sigma_x^{i+1} \approx \left(\sigma_x^i \sigma_x^{i+1} + \sigma_y^i \sigma_y^{i+1}\right)/2$ in the rotating wave approximation (neglecting strongly off-resonant couplings). Then the total Hamiltonian of the superconducting circuit proposed to emulate the dynamics of the Holstein model $H_{\rm sim} = \sum_{i=1}^{N} \left\{ H_{\rm q}^i + H_{\rm coup}^i + H_{\rm q-osc}^i + H_{\rm osc}^i \right\}$ in the new basis is given by

$$H_{\rm sim} \approx \frac{1}{2} \sum_{i=1}^{N-1} g_i(\Delta_{ii+1}^c) \left[\sigma_x^i \sigma_x^{i+1} + \sigma_y^i \sigma_y^{i+1} \right] + \sum_{i=1}^{N} \left\{ \frac{\Delta_i}{2} \sigma_z^i + \eta_i \sigma_z^i \left(c_i^\dagger + c_i \right) + \hbar \omega_i' c_i^\dagger c_i \right\} . \tag{4}$$

Comparison of the Hamiltonians (3) and (4), demonstrates that a chain of coupled flux qubits with a single quantum LC oscillator coupled to each qubit can simulate the same dynamics of the Holstein model with Δ_i, $g_i(\Delta_{ii+1}^c)$, η_i, ω_i' corresponding to ϵ_n, V_n, κ_n, ω_n, respectively. Interestingly, for superconducting flux qubits, the couplings $g_i(\Delta_{ii+1}^c)$ and η_i are tunable. The implementable range of $g_i(\Delta_{ii+1}^c)$ is in the range of approximately zero to 1 GHz [38]. η_i can be in the $<$10 GHz range depending on the frequency of the resonator and Δ_i can be chosen between zero and 13 GHz [37]. The tunability and wide implementable range of these parameters makes it possible to study different parameter regimes of interest (strong coupling $\eta_i \gg g_i$, weak coupling $\eta_i \ll g_i$ and intermediate $\eta_i \sim g_i$ regimes) using the proposed quantum simulator.

Preparation of the qubits in their ground state is straightforward: One needs to allow them to relax as close as possible to their ground state by cooling them down to the dilution refrigerator ambient temperature. Subsequently, the qubits can be initialized by flux control in the appropriate initial states for the simulation. The excitation of a qubit is undemanding to achieve with the application of a resonant microwave excitation (π-pulse) carried by a microwave line which is connected to the respective qubit. This technique has been used extensively, e.g., for the observation of Rabi oscillations in a flux qubit [40,43]. After some evolution time the populations of the qubit states are measured.

3 Temperature

Note that the standard Holstein model discussed above is at zero Kelvin; however, the superconducting circuit (as a real physical system) is at finite temperature $T_{\rm sim}$. Currently, a superconducting circuit can be refrigerated down to a very low temperature, around 10 mK $\approx$ 0.2 GHz, and the flux qubits can be even cooled down far below 10 mK using active microwave cooling [44]. Although the quantum simulator being at finite temperature seems to be a disadvantage, we will see in the following that the easy tunability over $T_{\rm sim}$ allows one to investigate the physically relevant case of a finite temperature Holstein model over a wide range of temperatures. To this end, we will generalize the Standard Holstein Hamiltonian.

4 Generalized Holstein model

The Hamiltonian of multi-mode Holstein model is given by

$$H_{\rm gen} = \frac{1}{2}\sum_{\substack{n=1\\ n\neq m}}^{N}\sum_{m=1}^{N} V_{nm}\left(\sigma_x^n\sigma_x^m + \sigma_y^n\sigma_y^m\right) + \sum_{n=1}^{N}\left\{\frac{\epsilon_n}{2}\,\sigma_z^n + \sum_k\left[\kappa_{nk}\,\sigma_z^n\left(b_{nk}^\dagger + b_{nk}\right) + \hbar\omega_{nk}\,b_{nk}^\dagger b_{nk}\right] + \mathcal{C}_n\right\}, \quad (5)$$

where k labels the vibrational modes coupled to the site n with frequency ω_{nk}, $\kappa_{nk} = \hbar\omega_{nk}\sqrt{R_{nk}}$ is the coupling of the electronic excitation of the site n to the vibrational mode k with R_{nk} being the dimensionless Huang-Rhys factor (electron–phonon coupling constant) [45], and constant $\mathcal{C}_n = \sum_k \hbar\omega_{nk}R_{nk} + D_n$ with D_n being the gas-to-crystal shift of the transition energy due to nonresonant forces [45,46]. Since a constant energy offset does not alter the dynamics, we ignore $\mathcal{C}_n$ in our approach. Now each site couples to a set of oscillators with frequencies ω_{nk} and corresponding couplings κ_{nk}. We have also generalized interactions V_{nm} between arbitrary sites. The dynamics of a multiple-mode Holstein model can be reproduced by a similar superconducting circuit shown in Fig. 2 with additional quantum LC oscillators coupled to each flux qubit; see Fig. 3a.

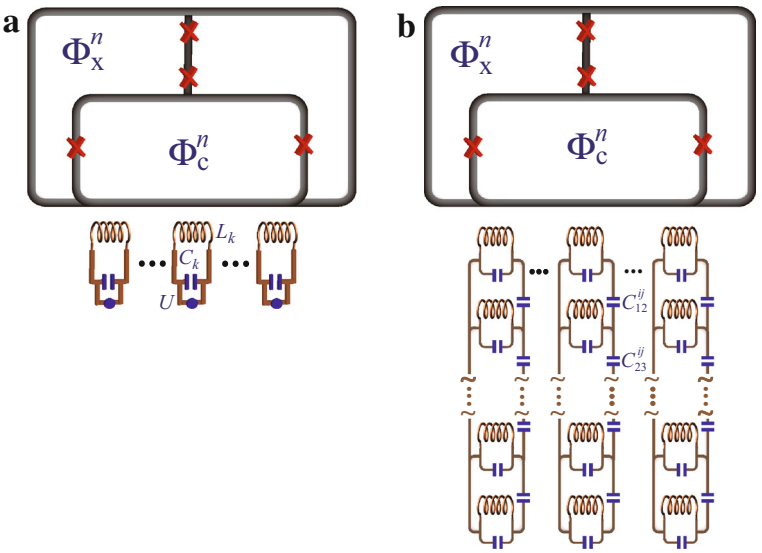

Fig. 3 Representation of a single flux qubit coupled to quantum LC oscillators. **a** Many single resonators are directly coupled to the qubit. **b** Using a linear-algebraic bath transformation [48], the set of independent resonators (directly coupled to the qubit) are transformed into a set of weakly coupled multiple parallel chain of resonators

The experimental implementation of such a quantum simulator can face challenges due to the current constraints in the realizable superconducting circuits. The number of quantum LC oscillators, that are directly coupled to a qubit is limited by the physical size of the superconducting qubits. Moreover, the coupling strength of the qubit to the quantum oscillator η_{ij} is limited and should not exceed a certain percentage of the frequency of the oscillator [47]. This coupling strength is given by $\eta_{ij}/\hbar\omega'_{ij} \approx \sqrt{L_r^{ij}\,(\beta_{ij}\,I_p^{ij})^2/2\hbar\,\omega'_{ij}}$ and can be numerically simplified to

$$\frac{\eta_{ij}}{\hbar\,\omega'_{ij}} = \sqrt{R_{ij}} = \frac{5.48\,\beta_{ij}\,I_p^{ij}}{50\,\mathrm{nA}}\left(\frac{Z_r^{ij}}{100\,\Omega}\right)^{1/2}\left(\frac{\omega'_{ij}}{2\pi\ \mathrm{GHz}}\right)^{-1}. \tag{6}$$

Here β_{ij} is dimensionless inductive coupling strength, corresponding to the inductive division ratio (flux of the j-th oscillator coupled to the i-th qubit is β_{ij} times of the qubit flux). This parameter needs to be far below 1 to avoid hybridizing the qubit with the resonator. L_r^{ij} is the inductance of the resonator, Z_r^{ij} is the oscillator impedance and has to be well below the impedance of free space (not much higher than 100 Ω), in order to maintain high-quality factors for the resonators. I_p^{ij} is the effective persistent current of the DC superconducting quantum interference device (SQUID) loop, which is the linear slope of the qubit energy splitting with respect to DC SQUID flux. In principle, I_p^{ij} can be made large, though this would also increase the linear sensitivity of the qubit energy to the flux noise correspondingly.

These challenges can be addressed and resolved by a linear-algebraic bath transformation [48] that we have proposed recently—more details are provided in "Appendix 1". Based on a simple linear-algebraic approach, the set of independent LC oscillators directly coupled to a qubit, Fig. 3a, can be transformed into a set of weakly coupled multiple parallel chain of oscillators; see Fig. 3b. This transformation can dramatically reduce the number of the oscillators that are directly coupled to the qubit as well as the coupling strength of the quantum oscillators to the qubit. To specify the number of the required resonators and their parameters and to feature outrunning classical algorithms with our proposed approach, as an example, here we study the feasibility and provide an outlook for the emulation of the dynamics of the chlorosome light-harvesting antenna from green sulfur bacteria.

5 Chlorosome light-harvesting antennae

The green sulfur bacteria live in a deep sea where only a few hundred photons per second arrive at a bacterium [49]. Amazingly, they are able to transfer the photon energy efficiently, rapidly, and robustly to the reaction center to generate the electrochemical potential energy gradient and exploit it in the photosynthetic metabolic cycle. Compared with other light-harvesting species, the chlorosome, which is the antenna complex of green sulfur bacteria, has a unique feature. It is composed of 200–250 thousands bacteriochlorophyll molecules organized into supramolecular assembly [50,52]. How the quantum dynamics helps the excitation energy transfer within this giant

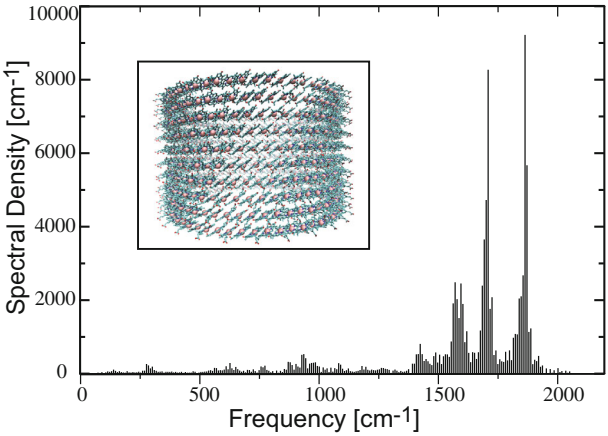

Fig. 4 Spectral density of the electron–phonon coupling of bacteriochlorophyll molecules in the chlorosome antenna of green sulfur bacteria with 253 phonon modes. The spectral density of the phonon bath was obtained from a quantum mechanics/molecular mechanics (QM/MM) simulation with time-dependent density functional theory in Ref. [17]. An experimentally resolved [52] structure of the chlorosome is shown in the *inset*

molecular aggregate is an interesting question and has attracted many research groups, see the references cited in Refs. [17,18,50,51]. The structure model of the chlorosome has been proposed from experiments [52] and studied theoretically by some of the authors [17,18,53] with combining colored noise stochastic open quantum propagation model of the exciton dynamics and a quantum mechanics/molecular mechanics (QM/MM) simulation with time-dependent density functional theory to take the atomistic details of the environmental bath fluctuation into account. Figure 4 demonstrates the theoretically obtained spectral density [17,18] of the electron–phonon coupling of bacteriochlorophyll molecules in the chlorosome antenna of green sulfur bacteria with 253 phonon modes coupled to each electronic state.

The single-exciton transfer dynamics of the chlorosome can be described by the multi-mode Holstein model given by Eq. (5). As mentioned in the introduction, numerically exact approaches (for example, the HEOM approach) for simulating the non-Markovian dynamics of this model can be obtained for only small systems ($<$20 sites) with a limited number of bath modes; see Fig. 1. However, this Hamiltonian can be emulated by an analog quantum simulator consist of chain of superconducting qubits and 253 quantum LC oscillators coupled to each qubit. The size of each flux qubit is around tens to hundreds of microns and there is no enough physical space to couple it directly to 253 resonators. We can reduce number of the resonators that are directly coupled to the qubit by using the linear-algebraic bath transformation [48], see "Appendix 1" for more details. This transformation mixes resonator modes with different frequencies to distributes 253 modes to, for example, a set of 6 parallel chains of quantum resonators, Fig. 3b, with each chain having at most 43 coupled oscillators. In addition to reducing number of the resonators that are directly coupled to the qubit, this mapping will also reduce the required coupling strength of the qubit to the primary oscillator modes (the first oscillators in the chains that are directly coupled to the qubit).

Note that the parameters of the superconducting simulator are temperature dependent. To account for finite temperature, we first transform the spectral density given in Fig. 4 using $C(\omega, T) = \{1 + \coth[\hbar\omega/(2k_B T)]\} J^{\mathrm{A}}(\omega)$, where the subscript "A" denotes the antisymmetric spectral density $J^{\mathrm{A}}(\omega) = J(\omega)$ if $\omega \geq 0$; and $J^{\mathrm{A}}(\omega) = -J(-\omega)$ if $\omega < 0$, see [27] for more details. Since the chlorosome is at room temperature, $T_{\mathrm{ch}} = 300$ K, and the superconducting circuit can be considered at T_{sim}=10 mK, then all the parameters of the quantum simulator need to be rescaled accordingly; $\mathcal{A}_{\mathrm{sim}} = (T_{\mathrm{sim}}/T_{\mathrm{ch}})\,\mathcal{A}_{\mathrm{ch}}$, with $\mathcal{A}_{\mathrm{sim}}$ and $\mathcal{A}_{\mathrm{ch}}$ indicating any parameter of the quantum simulator and chlorosome, respectively. Then after rescaling, we perform the linear-algebraic bath transformation. With this procedure, the coupling strengths between the qubit and the oscillators that are directly coupled to the qubit, Fig. 3b, need to be around 150–210 MHz. The coupling between the oscillators in the chains are around 100–560 MHz, the required frequencies for the quantum oscillators are around 1.4–1.6 GHz. The resonators here need to have high-quality factors.

6 Discussion

We have shown that it is appealing to simulate the dynamics of open quantum systems with complex environments and structured spectral densities (such as, the chlorosome or the examples given in Fig. 1) by using a chain of few tens of coherent qubits. In our previous work [27], we presented a detailed study on simulating the dynamics of Fenna–Matthews–Olson photosynthetic complex as an example of complex open quantum systems. The main focus of current manuscript has been to address the limit that analog quantum simulators based on superconducting circuits with precisely engineered quantum environment may outperform exact classical computational approaches, such as the HEOM approach, allowing us to study non-Markovian effects. Furthermore, here we have discussed the simulation of standard, as well as, generalized Holstein model at finite temperature which has many applications in molecular aggregates, polymers, and superconductivity. Using the linear-algebraic bath transformation, we will be able to simulate dynamics of complex open quantum systems with thousands of phonon modes. Such a simulation is as exact as numerical approaches such as HEOM and definitely out of reach of any currently available computational device.

As mentioned in the introduction, a similar idea based on superconducting circuit QED [35] has been proposed earlier to simulate the standard Holstein model. In the above proposal the coupling of the oscillator to the qubit is achieved in the large-detuning, dispersive limit of a transverse interaction, and in a rotating, dressed frame where the resonator is strongly driven. This gives a force on the oscillator in the second order in the interaction, which can only be large for very small dressed frequencies, and cannot be tuned all the way to zero. It has, in principle, the advantage that one can go to arbitrarily low mode frequencies without needing to actually engineer low-frequency modes. However, the requirement for constant, strong driving of the system is likely to encounter many experimental problems. In this scheme, the hopping is adjusted using flux-tunable SQUIDs in between the transmons. This means that none of these couplings can be tuned to zero. Furthermore, as the coupling between transmons is

reduced, the plasma frequency of the SQUIDs are as well, and this mode will start to be spuriously excited by the strong driving field. By contrast, in our scheme, the force on the bath modes is the result of first-order, static longitudinal interaction, which can be made strong without the need for any driving, can be tuned all the way to zero, and allows for structured spectral densities to be engineered, which has been the main focus of this paper. Also, the site hopping can be tuned all the way to zero simply by adjusting the couplers appropriately. This has been described earlier in Ref. [54].

Acknowledgements We acknowledge DTRA Grant No. DTRA1-10-1-0046, AFOSR UCSD Grant No. FA9550-12-1-0046, Department of Energy Award No. DE-SC0008733 and Harvard FAS RC team for Odyssey computer resources. A.J.K. acknowledges the Assistant Secretary of Defense for Research and Engineering under Air Force Contract No. FA8721-05-C-0002. Opinions, interpretations, conclusions and recommendations are those of the author and are not necessarily endorsed by the United States Government.

Appendix 1: Linear-algebraic bath transformation

Open quantum system approach to the spin-boson model often approximates the environment as a collection of non-interacting harmonic oscillators. This is known as a star-bath model and can be graphically illustrated in a star configuration as shown in Fig. 5a. Linear-algebraic bath transformation [48] converts the star-bath model into a set of weakly coupled multiple parallel chains as shown in Fig. 5b. The multiple-chain bath model has a few primary bath oscillators that are directly coupled to the system (spins/qubits) and the remaining oscillators (secondary bath modes) are coupled to the primary bath modes in a chain. This model employs a simple linear-algebraic approach to reduce the system-bath coupling strength as well as the number of the oscillators that are directly coupled to the system.

To apply the linear-algebraic bath transformation we start by writing the $H_{\mathrm{el-ph}} + H_{\mathrm{ph}}$ in a compact form [18,55] and then finding a unitary transformation $\boldsymbol{U}_n \boldsymbol{U}_n^{\dagger} = I$ that satisfies the following conditions [48]:

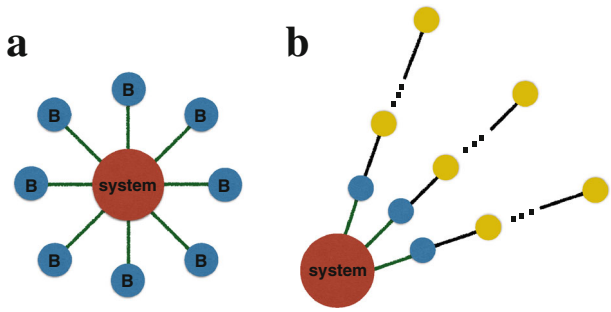

Fig. 5 **a** Star-bath model: Non-interacting quantum harmonic oscillators (shown in *blue*) are directly coupled to a system site (shown in *red*). **b** Multiple-chain bath model: A system site is coupled to multiple bath oscillator chains. In this model, the primary modes (shown in *blue*) are directly coupled to the system and the secondary modes (shown in *yellow*) are coupled to the primary bath modes in a chain (Color figure online)

$$H_{\text{el-ph}} + H_{\text{ph}} = \sum_n \left(L_n \ \mathbf{b}_n^\dagger \right) \mathbf{\Gamma}_n \begin{pmatrix} L_n \\ \mathbf{b}_n \end{pmatrix} = \sum_n \left(L_n^\dagger \ \tilde{\mathbf{b}}_n^\dagger \right) \tilde{\mathbf{\Gamma}}_n \begin{pmatrix} L_n \\ \tilde{\mathbf{b}}_n \end{pmatrix} \tag{7}$$

with

$$\mathbf{\Gamma}_n = \begin{pmatrix} \mathbf{0} & \boldsymbol{\kappa}_n^{\text{t}} \\ \boldsymbol{\kappa}_n & \mathbf{\Omega}_n \end{pmatrix}, \quad \tilde{\mathbf{\Gamma}}_n = \begin{pmatrix} \mathbf{0} & \tilde{\boldsymbol{\kappa}}_n^{\text{t}} \\ \tilde{\boldsymbol{\kappa}}_n & \tilde{\mathbf{\Omega}}_n \end{pmatrix} = \begin{pmatrix} \mathbf{1} & \mathbf{0}^{\text{t}} \\ \mathbf{0} & \boldsymbol{U}_n^\dagger \end{pmatrix} \mathbf{\Gamma}_n \begin{pmatrix} \mathbf{1} & \mathbf{0}^{\text{t}} \\ \mathbf{0} & \boldsymbol{U}_n \end{pmatrix}, \tag{8}$$

where $\tilde{\mathbf{b}}_n = \boldsymbol{U}_n^\dagger \mathbf{b}_n$ with $\mathbf{b}_n^\dagger$ ($\mathbf{b}_n$) being the N-dimensional creation (annihilation) operator vector of the phonons (oscillators). L_n is an operator that acts on the system, $\boldsymbol{\kappa}_n$ is the system-bath coupling strength vector, and $\mathbf{\Omega}_n$ is a diagonal matrix, which has the harmonic frequencies as the elements $\mathbf{\Omega}_n = \text{diag}(\omega_{n,1}, \ldots, \omega_{n,N})$. The first column of $\boldsymbol{U}_n$ is $\boldsymbol{\kappa}_n / ||\boldsymbol{\kappa}_n||_2$ and the other columns are given by the Gram-Schmidt process with random vectors [56]. $\tilde{\mathbf{\Gamma}}_n$ is a dense symmetric matrix and $\tilde{\boldsymbol{\kappa}}_n = (\tilde{\kappa}_{n,1}, 0, \ldots, 0)^{\text{t}}$ is the new system-bath coupling strength vector [48].

To complete the multiple-chain transformation, we introduce another unitary transformation $\tilde{\mathbf{U}}_n = \mathbf{P}_n \mathbf{U}_n$ that follows the following relations

$$\tilde{\mathbf{\Omega}}_n = \tilde{\mathbf{U}}_n^\dagger \mathbf{\Omega}_n \tilde{\mathbf{U}}_n \quad \text{and} \quad \tilde{\boldsymbol{\kappa}}_n = \tilde{\mathbf{U}}_n^\dagger \boldsymbol{\kappa}_n \, . \tag{9}$$

The permutation matrix $\mathbf{P}_n$ is used to rearrange the non-interacting bath oscillators as multiple groups of several interacting oscillators $\tilde{\mathbf{b}}_n = \tilde{\boldsymbol{U}}_n^\dagger \mathbf{b}_n$. Note that $\mathbf{U}_n$ is block diagonal and does not allow the interaction between oscillators from different groups. Now by choosing the l-th subblock $\mathbf{U}_n^{(l)}$ to be $\mathbf{g}_n^{(l)} / ||\mathbf{g}_n^{(l)}||_2$, we can define the primary modes (the ones that are directly coupled to the system sites) as collective oscillator modes. Here $\mathbf{g}_n$ is the rearranged coupling strength vector

$$\mathbf{g}_n = \mathbf{P}_n^\dagger \boldsymbol{\kappa}_n = \begin{pmatrix} \mathbf{g}_n^{(1)} \\ \vdots \\ \mathbf{g}_n^{(N_{\text{eff}})} \end{pmatrix}, \tag{10}$$

and N_{eff} is the number of groups of oscillators. The final step is to tridiagonalize the l-th subblock $\tilde{\mathbf{\Omega}}_n^{(l)}$ using the Hessenberg transform [56] via the Householder procedure $\tilde{\mathbf{\Omega}}_n^{(l)} = \mathcal{T}^{(l)} \, \mathbf{\Xi}^{(l)} \mathcal{T}^{(l)\dagger}$. The diagonal elements of the tridiagonal matrix $\mathbf{\Xi}^{(l)}$ represent the frequencies of the transformed bath modes and its off-diagonal elements are the coupling strengths between the oscillators in the chain model. $\mathcal{T}^{(l)}$ is a Hessenberg unitary transform matrix that keeps the primary bath mode unchanged. To adjust the system-bath coupling strengths of primary modes within the experimentally realizable parameter domain, we have also developed a bath mode partitioning scheme [48]. The scheme is called leaping partition (LP), which selects the oscillators far away from each other to form multiple parallel chains. For example, we grouped 253 oscillators of chlorosome into 6 groups as

$$\{\omega_1, \omega_{1+6}, \omega_{1+12}, \cdots, \omega_{1+252}\}, \quad \{\omega_2, \omega_{2+6}, \omega_{2+12}, \cdots, \omega_{2+246}\},$$
$$\{\omega_3, \omega_{3+6}, \omega_{3+12}, \cdots, \omega_{3+246}\}, \quad \{\omega_4, \omega_{4+6}, \omega_{4+12}, \cdots, \omega_{4+246}\},$$
$$\{\omega_5, \omega_{5+6}, \omega_{5+12}, \cdots, \omega_{5+246}\}, \quad \{\omega_6, \omega_{6+6}, \omega_{6+12}, \cdots, \omega_{6+246}\}, \tag{11}$$

where $\omega_l \leq \omega_m$ if $l \leq m$. See Ref. [48] for more examples on the rearrangement of the oscillators and also the MATLAB code that we have used for the transformation.

Appendix 2: Hierarchically equations of motion approach

In order to estimate the treatable system size for the Holstein model on classical computers we run benchmark calculations with *QMaster*, which is a high-performance implementation of the hierarchically coupled equations of motion approach (HEOM) [19,57,58]. HEOM is based on an open quantum system approach and treats the phonon modes as continuum bath.

The time evolution of the total system, described by the density operator $R(t)$ is given by the Liouville equation

$$\frac{\mathrm{d}}{\mathrm{d}t}R(t) = -\frac{\mathrm{i}}{\hbar}[\mathcal{H}(t), R(t)] = -\frac{\mathrm{i}}{\hbar}\mathcal{L}(t)R(t). \tag{12}$$

At initial time $t_0 = 0$ we assume that the density operator $R(t_0) = \rho(t_0) \otimes \rho_{\mathrm{phon}}(t_0)$ factorizes into the system degrees of freedom, described by the reduced density operator $\rho(t)$, and vibrational degrees of freedom $\rho_{\mathrm{phon}}(t)$. The dynamics of the reduced density operator is then obtained by averaging out the vibrational degrees of freedom

$$\rho(t) = \langle \mathrm{T}_+ \exp\Big(-\frac{\mathrm{i}}{\hbar}\int_0^t \mathrm{d}s\, \mathcal{L}(s)\Big)\rangle \rho(0). \tag{13}$$

We employ a high-temperature approximation $\hbar\gamma_m / k_{\mathrm{B}}T < 1$ and parameterize the spectral density as a sum over N_{peaks} shifted Drude–Lorentz peaks

$$J(\omega) = \sum_{k=1}^{N_{\mathrm{peaks}}} \left(\frac{\nu_k \lambda_k \omega}{\nu_k^2 + (\omega + \Omega_k)^2} + \frac{\nu_k \lambda_k \omega}{\nu_k^2 + (\omega - \Omega_k)^2} \right). \tag{14}$$

The time non-local equation can then be cast into a hierarchy of coupled time local equations of motion for a set of auxiliary matrices $\sigma^{\vec{n}}$

$$\frac{\mathrm{d}}{\mathrm{d}t}\sigma^{\vec{n}}(t) = -\frac{\mathrm{i}}{\hbar}[\mathcal{H}_{\mathrm{ex}}, \sigma^{\vec{n}}(t)] - \sum_{m,k=1,s=\pm 1}^{N,N_{\mathrm{peaks}}} \frac{2}{\beta\hbar^2} \frac{\lambda_k \nu_k}{(\gamma_1 + \mathrm{i}s\Omega_k)^2 - \nu_k^2} V_m^{\times} V_m^{\times} \sigma^{\vec{n}}(t)$$

$$- \sum_{m,k=1,s=\pm 1}^{N,N_{\text{peaks}}} n_{m,k,s}(\nu_k + s\,\mathrm{i}\Omega_k)\sigma^{\vec{n}}(t)$$
$$+ \sum_{m,k=1,s=\pm 1}^{N,N_{\text{peaks}}} \left[\frac{\mathrm{i}}{\hbar} V_m^{\times} \sigma^{\vec{n}^{+}_{m,k,s}}(t) + \theta_{m,k,s}\sigma^{\vec{n}^{-}_{m,k,s}}(t) \right], \tag{15}$$

Here we define $\vec{n} = (n_{1,1,+}, n_{1,1,-}, \ldots, n_{1,M,+}, n_{1,M,-}, \ldots, n_{N,M,+}, n_{N,M,-})$, $V_m^{\times}\sigma = [a_m^{\dagger}a_m, \sigma]$, $V_m^{\circ}\sigma = [a_m^{\dagger}a_m, \sigma]_+$ and $\theta_{m,k,s} = \frac{\mathrm{i}}{2}\left(\frac{2\lambda_k}{k_B T\hbar} V_m^{\times} - \mathrm{i}\lambda_k(\nu_k + s\,\mathrm{i}\Omega_k)V_m^{\circ} - \frac{2\lambda_k}{\beta\hbar^2}\frac{(\nu_k + \mathrm{i}s\Omega_k)^2}{\gamma_1^2 - (\nu_k + \mathrm{i}s\Omega_k)^2} V_m^{\times}\right)$. The reduced density matrix is given as $\rho(t) = \sigma^{\vec{0}}(t)$. The hierarchy Eq. (15) can be truncated for a sufficiently large hierarchy depth $\sum_{m,k=1,s=\pm 1}^{N,N_{\text{peaks}}} n_{m,k,s} \geq N_{\max}$, for which convergence is tested by comparing the dynamics for different truncation levels $N_{\max}$.

Appendix 3: Computational details to estimate the treatable system size

Solving the hierarchy Eq. (15) for a large system size is challenging, and requires a considerable amount of computational resources, both in memory and number of floating point operations per second (FLOPS). The whole set of auxiliary matrices needs to be retained in the CPU memory during the complete propagation of the exciton dynamics, and all entries need to be update for each propagation step. The total number of auxiliary matrices $N_\sigma = (2\,N_{\text{peaks}}\,N + N_{\max})!/(N_{\max}!(2\,N_{\text{peaks}}\,N)!$ depends on the number of sites N in the Holstein Model (see Eq. (4), main text), the truncation level $N_{\max}$ and the number of peaks in the spectral density N_{peaks}. The factor $2\,N_{\text{peaks}}$ takes into account the shifts of the peaks in the spectral density, Eq. (14) in positive as well as in negative direction along the frequency axis. Thus, for the parameters used to perform the benchmark calculations in Fig. 1 of the main text, we need to propagate up to several millions of auxiliary matrices in log-step, see Table 1.

We carry out the calculations with the help of a sophisticated algorithm provided by the *QMaster* package [16]. *QMaster* is based on massively parallelized vector streaming. The idea behind the algorithm is to efficiently distribute the workload among the available computational units while keeping up a high memory bandwidth. The latter is achieved by a suitable layout of how the auxiliary matrices are stored in the CPU memory. In general *QMaster* also runs on GPUs and the XeonPhi accelerator. However, todays available GPU memory is limited to 24GB (K80) which is the reason why we run the benchmark calculations on a 64-core AMD Opteron processor with 256 GB memory. *QMaster* is a single-device implementation, since distributed computation among multiple compute nodes connected by Ethernet is rendered inefficient, due to the large communication overhead [23]. More information about the algorithm as well es a performance analysis are given elsewhere [16].

Table 1 summarizes the technical aspects of the underlying computations to estimate the treatable system size (Fig. 1, main text). The propagation is performed over 10

Table 1 Benchmarks of the treatable system size with respect to the number of sites and number of peaks in the spectral density

N	N_{peaks}	#σ-matrices	Used memory σ-matrices (GB)	Compuation time (min)
14	11	4,965,115	87	6.3
21	7	4,322,340	170	14.5
42	2	818,805	129	16.5
93	1	142, 880	110	30.8
100	1	176,851	158	41.0

The calculations are run with the high-performance HEOM-implementation provided by *QMaster*. Computation time (without initialization) corresponds to the propagation of 10 time steps with truncation level $N_{\text{max}} = 3$. The parameter $N_{\text{peaks}} = 1$ describes a non-shifted Drude–Lorentz spectral density ($\Omega = 0$). The exciton propagation is based on fourth-order Runge–Kutta integrator and run on a 64-core AMD Opteron processor with 250 GB memory

time steps for a given electronic excitation at t_0. The truncation level is set to $N_{\text{max}} = 3$ which has proven as reasonable value for several light-harvesting complexes [15,16,23,59]. Shown are the results for the maximal treatable system sizes with respect to the number of sites and number of peaks in the spectral density. Once one more peak is added *QMaster* needs to allocate more than 250 GB of memory, and therefore terminates with a segmentation fault. Thus memory consumption sets the hard limit for the treatable system size. The computation time is a somewhat more soft criteria, since the total computation time depends on the number of propagation steps which strongly depends on the system at hand. For example, calculations for a quadrant of the PSII-supercomplex comprising of 93 sites have been carried out for which the exciton dynamics was propagated over 20,000 time steps with a time increment of 5 fs (100 ps total propagation time) [59]. According to Table 1, the calculations for a non-shifted Drude–Lorentz peak takes about 43 days of total computation time, which allows at least to run simulations to test the convergence of the hierarchy with respect to the truncation level [59].

References

1. Alexandrov, A.S., Mott, N.F.: Polarons and Bipolarons. World Scientific, Singapore (1995)
2. Freericks, J.K., Jarrell, M., Scalapino, D.J.: Holstein model in infinite dimensions. Phys. Rev. B **48**, 6302 (1993)
3. Ciuchi, S., de Pasquale, F., Fratini, S., Feinberg, D.: Dynamical mean-field theory of the small polaron. Phys. Rev. B **56**, 4494 (1997)
4. Bonča, J., Trugman, S.A., Batistić, I.: Holstein polaron. Phys. Rev. B **60**, 1633 (1999)
5. Romero, A.H., Brown, D.W., Lindenberg, K.: Exact weak-coupling radius of the Holstein polaron in one, two, and three dimensions. Phys. Lett. A **254**, 287 (1999)
6. Romero, A.H., Brown, D.W., Lindenberg, K.: Polaron effective mass, band distortion, and self-trapping in the Holstein molecular-crystal model. Phys. Rev. B **59**, 13728 (1999)
7. Romero, A.H., Brown, D.W., Lindenberg, K.: Effects of dimensionality and anisotropy on the Holstein polaron. Phys. Rev. B **60**, 14080 (1999)
8. Hoffmann, M., Soos, Z.G.: Optical absorption spectra of the Holstein molecular crystal for weak and intermediate electronic coupling. Phys. Rev. B **66**, 024305 (2002)

9. Barišić, O.S.: Calculation of excited polaron states in the Holstein model. Phys. Rev. B **69**, 064302 (2004)
10. Spencer, P.E., Samson, J.H., Kornilovitch, P.E., Alexandrov, A.S.: Effect of electron–phonon interaction range on lattice polaron dynamics: a continuous-time quantum Monte Carlo study. Phys. Rev. B **71**, 184310 (2005)
11. Berciu, M.: Green's function of a dressed particle. Phys. Rev. Lett. **97**, 036402 (2006)
12. Goodvin, G.L., Berciu, M., Sawatzky, G.A.: Green's function of the Holstein polaron. Phys. Rev. B **74**, 245104 (2006)
13. Prokof'ev, N.V., Svistunov, B.V.: Bold diagrammatic Monte Carlo: a generic sign-problem tolerant technique for polaron models and possibly interacting many-body problems. Phys. Rev. B **77**, 125101 (2008)
14. Kreisbeck, C., Kramer, T., Rodríguez, M., Hein, B.: High-performance solution of hierarchical equations of motion for studying energy transfer in light-harvesting complexes. J. Chem. Theory Comput. **7**, 2166 (2011)
15. Kreisbeck, C., Kramer, T.: Long-lived electronic coherence in dissipative exciton-dynamics of light-harvesting complexes. J. Phys. Chem. Lett. **3**, 2828 (2012)
16. Kreisbeck, C., Kramer, T., Aspuru-Guzik, A.: Scalable high-performance algorithm for the simulation of exciton dynamics. Application to the light-harvesting complex II in the presence of resonant vibrational modes. J. Chem. Theory Comput. **10**, 4045 (2014)
17. Fujita, T., Brookes, J.C., Saikin, S.K., Aspuru-Guzik, A.: Memory-assisted exciton diffusion in the chlorosome light-harvesting antenna of green sulfur bacteria. J. Phys. Chem. Lett. **3**, 2357 (2012)
18. Fujita, T., Huh, J., Saikin, S.K., Brookes, J.C., Aspuru-Guzik, A.: Theoretical characterization of excitation energy transfer in chlorosome light-harvesting antennae from green sulfur bacteria. Photosynth. Res. **120**, 273 (2014)
19. Ishizaki, A., Fleming, G.R.: Unified treatment of quantum coherent and incoherent hopping dynamics in electronic energy transfer: Reduced hierarchy equations approach. J. Chem. Phys. **130**, 234111 (2009)
20. Ishizaki, A., Fleming, G.R.: Theoretical examination of quantum coherence in a photosynthetic system at physiological temperature. Proc. Natl. Acad. Sci. USA **106**, 17255 (2009)
21. Strunz, W.T., Diósi, L., Gisin, N.: Open system dynamics with non-Markovian quantum trajectories. Phys. Rev. Lett. **82**, 1801 (1999)
22. Süß, D., Eisfeld, A., Strunz, W. T.: Hierarchy of stochastic pure states for open quantum system dynamics. arXiv:1402.4647 (2014)
23. Strümpfer, J., Schulten, K.: Light harvesting complex II B850 excitation dynamics. J. Chem. Phys. **131**, 225101 (2009)
24. Feynman, R.P.: Quantum mechanical computers. Found. Phys. **16**, 507 (1982)
25. Feynman, R.P.: Simulating physics with computers. Int. J. Theor. Phys. **21**, 467 (1986)
26. Buluta, I., Nori, F.: Quantum simulators. Science **326**, 108 (2009)
27. Mostame, S., Rebentrost, P., Eisfeld, A., Kerman, A.J., Tsomokos, D.I., Aspuru-Guzik, A.: Quantum simulator of an open quantum system using superconducting qubits: exciton transport in photosynthetic complexes. New J. Phys. **14**, 105013 (2012)
28. Nation, P.D., Johansson, J.R., Blencowe, M.P., Nori, F.: Colloquium: Stimulating uncertainty: Amplifying the quantum vacuum with superconducting circuits. Rev. Mod. Phys. **84**, 1 (2012)
29. Georgescu, I.M., Ashhab, S., Nori, F.: Quantum simulation. Rev. Mod. Phys. **86**, 153 (2014)
30. Herrera, F., Krems, R.V.: Tunable Holstein model with cold polar molecules. Phys. Rev. A **84**, 051401(R) (2011)
31. Herrera, F., Madison, K.W., Krems, R.V., Berciu, M.: Investigating polaron transitions with polar molecules. Phys. Rev. Lett. **110**, 223002 (2013)
32. Hague, J.P., MacCormick, C.: Quantum simulation of electron–phonon interactions in strongly deformable materials. New J. Phys. **14**, 033019 (2012)
33. Stojanovic, V.M., Shi, T., Bruder, C., Cirac, J.I.: Quantum simulation of small-polaron formation with trapped ions. Phys. Rev. Lett. **109**, 250501 (2012)
34. Mezzacapo, A., Casanova, J., Lamata, L., Solano, E.: Digital quantum simulation of the Holstein model in trapped ions. Phys. Rev. Lett. **109**, 200501 (2012)
35. Mei, F., Stojanović, V.M., Siddiqi, I., Tian, L.: Analog superconducting quantum simulator for Holstein polarons. Phys. Rev. B **88**, 224502 (2013)

36. Stojanović, V.M., Vanevic, M., Demler, E., Tian, L.: Transmon-based simulator of nonlocal electron–phonon coupling: a platform for observing sharp small-polaron transitions. Phys. Rev. B **89**, 144508 (2014)
37. Paauw, F.G., Fedorov, A., Harmans, C.J.P.M., Mooij, J.E.: Tuning the gap of a superconducting flux qubit. Phys. Rev. Lett. **102**, 090501 (2009)
38. Niskanen, A.O., Harrabi, K., Yoshihara, F., Nakamura, Y., Lloyd, S., Tsai, J.S.: Quantum coherent tunable coupling of superconducting qubit. Science **316**, 723 (2007)
39. Ashhab, S., Niskanen, A.O., Harrabi, K., Nakamura, Y., Picot, T., de Groot, P.C., et al.: Interqubit coupling mediated by a high-excitation-energy quantum object. Phys. Rev. B **77**, 014510 (2008)
40. Clarke, J., Wilhelm, F.K.: Superconducting quantum bits. Nature **453**, 1031 (2008)
41. You, J.Q., Nori, F.: Atomic physics and quantum optics using superconducting circuits. Nature **474**, 589 (2011)
42. Bertet, P., Chiorescu, I., Burkard, G., Semba, K., Harmans, C.J.P.M., DiVincenzo, D.P., et al.: Dephasing of a superconducting qubit induced by photon noise. Phys. Rev. Lett. **95**, 257002 (2005)
43. Chiorescu, I., Nakamura, Y., Harmans, C.J.P.M., Mooij, J.E.: Coherent quantum dynamics of a superconducting flux qubit. Science **299**, 1869 (2003)
44. Valenzuela, S.O., Oliver, W.D., Berns, D.M., Berggren, K.K., Levitov, L.S., Orlando, T.P.: Microwave-induced cooling of a superconducting qubit. Science **314**, 1589 (2006)
45. Roden, J., Eisfeld, A., Dvořák, M., Bünermann, O., Stienkemeier, F.: Vibronic line shapes of PTCDA oligomers in helium nanodroplets. J. Chem. Phys. **134**, 054907 (2011)
46. Spano, F.C., Silvestri, L.: Multiple mode exciton-vibrational coupling in H-aggregates: synergistic enhancement of the quantum yield. J. Chem. Phys. **132**, 094704 (2010)
47. Kerman, A.J.: Quantum information processing using quasiclassical electromagnetic interactions between qubits and electrical resonators. New J. Phys. **15**, 123011 (2013)
48. Huh, J., Mostame, S., Fujita, T., Yung, M.H., Aspuru-Guzik, A.: Linear-algebraic bath transformation for simulating complex open quantum systems. New J. Phys. **16**, 123008 (2014)
49. Manske, A.K., Glaeser, J., Kuypers, M.M.M., Overmann, J.: Physiology and phylogeny of green sulfur bacteria forming a monospecific phototrophic assemblage at a depth of 100 meters in the black sea. Appl. Environ. Microbiol. **71**, 8049 (2005)
50. Oostergetel, G.T., van Amerongen, H., Boekema, E.J.: The chlorosome: a prototype for efficient light harvesting in photosynthesis. Photosynth. Res. **104**, 245 (2010)
51. Lambert, N., Chen, Y.-N., Cheng, Y.-C., Li, C.-M., Chen, G.-Y., Nori, F.: Quantum biology. Nat. Phys. **9**, 10 (2013)
52. Ganapathy, S., Oostergetel, G.T., Wawrzyniak, P.K., Reus, M., Gomez Maqueo Chew, A., Buda, F., et al.: Alternating syn-anti bacteriochlorophylls form concentric helical nanotubes in chlorosomes. Proc. Natl. Acad. Sci. **106**, 8525 (2009)
53. Sawaya, N.P.D., Huh, J., Saikin, S.K., Fujita, T., Aspuru-Guzik, A.: Fast delocalization leads to robust long-range excitonic transfer in a large quantum chlorosome model. Nano Lett. **15**, 1722 (2015)
54. Kerman, A.J., Oliver, W.D.: High-fidelity quantum operations on superconducting qubits in the presence of noise Phys. Rev. Lett. **101**, 070501 (2008)
55. Guo, C.: Using density matrix renormalization group to study open quantum systems. Ph.D. Thesis, Ludwig-Maximilians-Universität (2012)
56. Golub, G.H., van Loan, C.F.: Matrix Computations, 3rd edn. Johns Hopkins University Press, Baltimore (1996)
57. Tanimura, Y., Kubo, R.: Time evolution of a quantum system in contact with a nearly Gaussian–Markoffian noise bath. J. Phys. Soc. Jpn. **58**, 101 (1989)
58. Tanimura, Y.: Reduced hierarchy equations of motion approach with Drude plus Brownian spectral distribution: probing electron transfer processes by means of two-dimensional correlation spectroscopy. J. Chem. Phys. **137**, 22A550 (2012)
59. Kreisbeck, C., Aspuru-Guzik, A.: Efficiency of energy funneling in the photosystem II supercomplex of higher plants. Chem. Sci. **7**, 4174 (2016)